Trans. Phenom. Nano Micro Scales, 8(2): 89-98, Summer and Autumn 2020
DOI: 10.22111/tpnms.2020.35902.1199

ORIGINAL RESEARCH PAPER

Nanofabrication of Zinc Ferrite ($ZnFe_2O_4$) composites for biomedical application

Parastoo Khalili[1], Majid Farahmandjou[2,*]

[1]School of Architecture and Environmental Design, University of Science & Technology (IUST), Tehran, Iran
[2]Department of Chemistry, Faculty of Pharmaceutical Sciences, Tehran Medical Sciences, Islamic Azad University, Tehran, Iran

Received 27 September 2020; revised 9 October 2020; accepted 10 October 2020; available online 10 November 2020

ABSTRACT: Today, green synthesis method for manufacturing of the nanoparticles (NPs) is the common rout for biomedical application. In this article, $ZnFe_2O_4$ NPs are fabricated by solgel method in the presence of surfactants. The samples are studied by x-ray diffraction (XRD), high resolution transmission electron microscopy (HRTEM), field effect scanning electron microscopy (FESEM), vibrating sample magnetometer (VSM), x-ray fluorescence (XRF) and fourier transform infrared spectroscopy (FTIR). The XRD results show hexagonal wurtzite structure of ZnO and spinel phase of rhombohedral α-Fe_2O_3. The crystallite size of annealed samples are calculated around 57 nm. The SEM images show that the NPs change from rod-shape to nanoparticle clusters of $ZnFe_2O_4$ by increasing temperature after annealing. The TEM studies show the formation of Fe_2O_3 shell around NPs with a diameter of 10 nm for as-prepared samples. The sharp peaks in FTIR spectrum indicate the stretching vibrations of Fe and Zn groups in the frequencies of 675 cm^{-1}, 602 cm^{-1} and 476 cm^{-1}. The results of magnetic measurements show coercive field and saturation magnetism around 2298 G and 34 memu/g respectively, for as-prepared samples. The XRF analysis demonstrate the decreasing of the Fe weight percent from 41.28 %Wt. to 39.64 %Wt., by increasing temperature.

KEYWORDS: *Nanorods; Optical properties; VSM; XRD; Zinc ferrite.*

INTRODUCTION

Metal oxide semiconductors (MOS) has many attractions due to its capability in the electronic and biomedical applications [1-8]. Recently, the production of metal oxide nanoparticles by green chemistry, including environmentally friendly methods, has dramatically increased [9-25]. In the last decade, the potential of metal-oxide nanoparticles for biomedical applications due to their antimicrobial, electronic and catalytic properties has been identified [26-35].

MRI (magnetic resonance imaging) contrast agent is the most important applications of ferrite (Fe_2O_4) NPs in biomedical and hospital engineering applications [36-43]. In recent years, ferrites doped with cations such as Mg, Mn, Zn, Ni, and Co have been extensively studied for applications as MRI contrast [44-52]. Coupled semiconductors such as zinc ferrite ($ZnFe_2O_4$), have been shown to increase the charge separation of electron-hole pairs, which increases the lifetime of the charge carriers [53]. This is based on the fact that the photo-generated electrons can flow from one semiconductor with a higher to a lower conduction band minimum [54-57]. The greatest advantage of $ZnFe_2O_4$ over other metal oxides is the ability to absorb a wide range of solar spectrum and compatibility with human body [58-70].

As a result, the efficiency of semiconductors improved, ZnO has almost the same band gap energy (3.2 eV), the biomedical capability is expected to be similar to that of oth-er semiconductors.

Based on these factors, synthesis of $ZnFe_2O_4$ and characterization of its structural and optical properties is very important.

Zinc ferrite NPs acquire a great deal of care in nanomedicine due to the lower toxicity of Zn^{2+} [71] Biomedical applications of $ZnFe_2O_4$ NPs are important among all kinds of ferrites due to the compatibility of Zn^{2+} ions for human bodies [72]. $ZnFe_2O_4$ NPs has been recognized as a good candidate for magnetic resonance imaging contrast agents which is much compatible than any other materials [73].

Nuclear magnetic resonance (NMR) is used to characterize the particles for its application in MRI with the variation of factors like shape, monodispersity, size and magnetization [74].

In the present work, first we have manufactured the $ZnFe_2O_4$ NPs by solgel method and then study the structural, optical, magnetic and morphological properties. The novelty of this work is the synthesis of the $ZnFe_2O_4$ nanoparticles with new precursors and solvent and also improving of the coercive field by 2298 Oe.

EXPERIMENTAL RESULTS

$ZnFe_2O_4$ NPs were fabricated by solgel synthesis by iron sulfate and zinc sulfate precursors. At the beginning, 3g $FeSO_4.6H_2O$ was dissolved in 60 mL dionized water with

✉ *Corresponding Author Email: *farahmandjou@iautmu.ac.ir*
Tel.: +98(21)22340298; Note. This manuscript was submitted on September 27, 2020; approved on October 9, 2020; published online November 10, 2020.

Nomenclature

Greek Symbols

λ	X-ray wavelength
ϑ	Bragg angle
β	Line broadening at half the maximum intensity

Subscripts

VSM	Vibrating Sample Magnetometer
XRD	X-ray Diffraction
FESEM	Field Emission scanning electron Microscopy
TEM	Transmission Electron Microscopy
FTIR	Fourier Transform Infrared Spectroscopy
FWHM	Full-Width at Half-Maximum
XRF	X-ray Florescence

stirring at room temperature. After 10 min, 1g of Cetyl trimethylammonium bromide (CTAB) stabilizer was added to the solution.

Then 3g of $ZnSO_4.6H_2O$ precursor was added to the solution and after 5 min 0.25 g sodium borohydride was slowly added to the solution and after 10 min the temperature was increased to 85°C. The product were evaporated for 3 hours, cooled to room temperature and finally calcined at 550 °C for 3 hours.

The specification of the size, structure and optical properties of the as-synthesis and annealed NPs were carried out. XRD was used to identify the crystalline phase and to estimate the crystalline size.

The XRD pattern were recorded with 2θ in the range of 4-85o with type X-Pert Pro MPD, Cu-Kα: λ = 1.54 Å. The morphology was characterized by FESEM with type KYKY-EM3200, 25 kV and TEM with type Zeiss EM-900, 80 kV. FTIR with WQF 510. Magnetic measurements were carried out using VSM with type VSM 7400 Lake Shore at room temperature.

RESULTS AND DISCUSSION

Figure 1 shows the x-ray diffraction (XRD) spectra of the samples.

Figure 1a shows the as-prepared sample with amorphous structure and figure 1b shows annealed one. The exhibited peaks correspond the α-Fe_2O_3 and ZnO NPs clearly show all the diffraction peaks of rhombohedral α-Fe_2O_3 and hexagonal wurtzite ZnO, respectively.

The peaks formed at 2θ angles of 31.92°, 34.61°, 36.36°, 47.46°, 56.67°, 62.69°, 66.33°, 68.08°, 69.19° and 72.68° are correspond to the diffraction peaks at (100), (002), (101), (102), (110), (103), (200), (112), (201) and (004) respectively, represent the hexagonal wurtzite in zinc oxide (JCPDS Card No. 89-0510).

This process is of the same kind for 24.15°, 33.02°, 35.56°, 40.80°, 49.37°, 53.96°, 57.45°, 62.22° and 63.95° which are indexed the diffraction peaks at (012), (104), (110), (113), (024), (300), (122), (214) and (300) respectively, suggesting the rhombohedral α-Fe_2O_3 structure (JCPDS Card No. 86-0550.

Moreover, peaks formed at 18.27°, 30.01°, 142.85°, 53.18°, 56.67° and 62.22° indicating the $ZnFe_2O_4$ structure (JCPDS Card No. 82-1049).

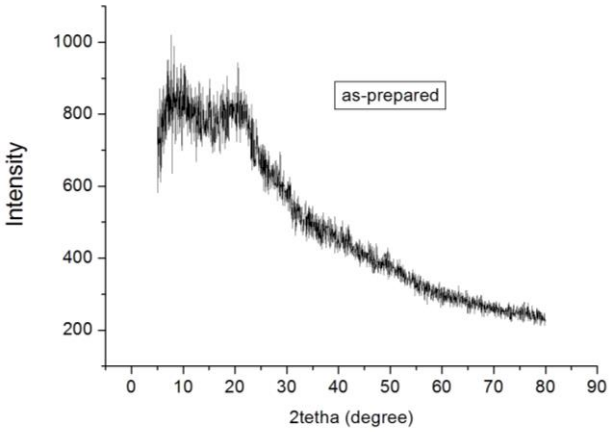

(a)

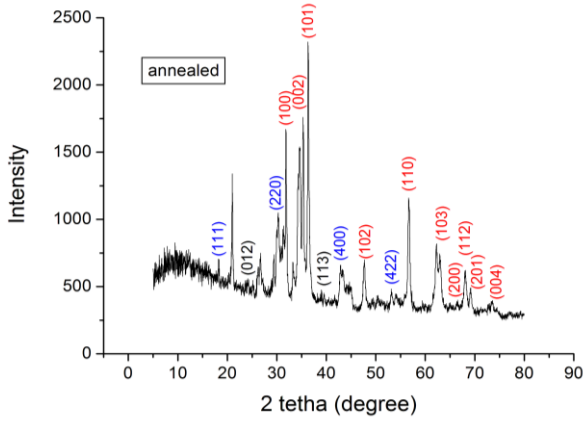

(b)

Fig. 1. XRD patterns of a) as-prepared and b) annealed Zinc ferrite samples

The crystallite size of the ordered $ZnFe_2O_4$ samples have been estimated from full width at half maximum (FWHM) and Debye-Sherrer formula according to equation the following [74]:

$$D = \frac{0.89\lambda}{\beta cos\theta} \quad (1)$$

where, 0.89 is the shape factor, λ is the x-ray wavelength, β is the line broadening at half the maximum intensity (FWHM) in radians, and θ is the Bragg angle. The crystallite size of as-prepared samples are determined around 50 nm while the annealed one are calculated about 57 nm from this

Debye-Sherrer equation. The XRD spectra also indicates the formation of $ZnFe_2O_4$ by increasing temperature after annealing. This should be caused by the enhanced interactions resulting from the extra Fe^{3+} ions in the sample.

Field emission scanning electron microscopy (FESEM) analysis of the as-prepared and annealed Zinc ferrite NPs was carried out to study the morphology of the samples. Figure 2(a) shows the SEM image of the as-prepared Zinc ferrite NPs and Figure 2(b) shows the SEM image of the annealed NPs at 550 ºC for 3 hours. The morphology of the samples show that the Zinc ferrite NPs change from rod-shape shape nanoparticle clusters of $ZnFe_2O_4$ by increasing temperature after annealing. With increasing temperature the size of the particles increases from 50 nm to 55 nm because of aggregation which is in accordance with XRD measurements.

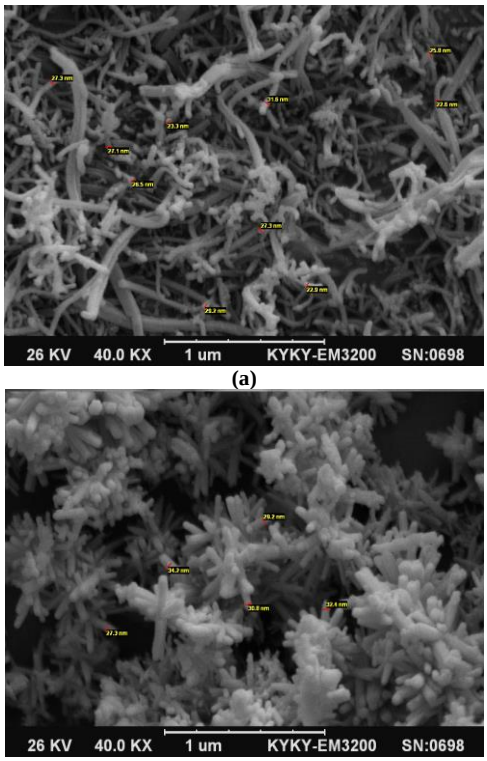

Fig. 2. FESEM images of the (a) as-prepared and (b) annealed Zinc ferrite NPs

It may be because of removing CTAB and sodium borohydride surfactants by annealing and changing the atomic and molecular interactions between NPs [76-88].

TEM analysis was carried out to measure the actual size of the samples and determine the exact shape of the NPs. Figure 3 shows the as-synthesized TEM image of squared-like Zinc ferrite with average diameter of 43 nm prepared by solgel synthesis route. TEM also shows the formation of $ZnFe_2O_4$ core-shell with the diameter of 10 nm Fe_2O_3 shell around NPs [89-102].

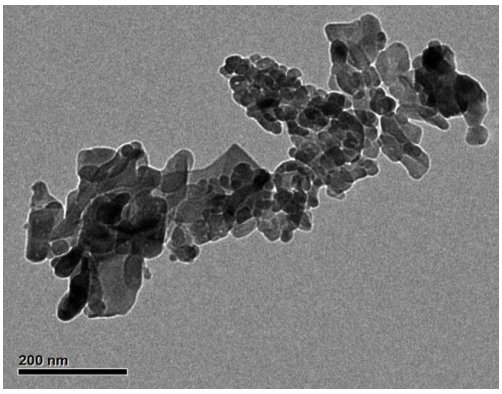

Fig. 3. HRTEM image of the as-prepared Zinc ferrite sample

Vibrating sample magnetometer (VSM) analysis of Zinc ferrite NPs prepared by solgel synthesis is shown in Figure 4 for as-synthesized samples and annealed one.

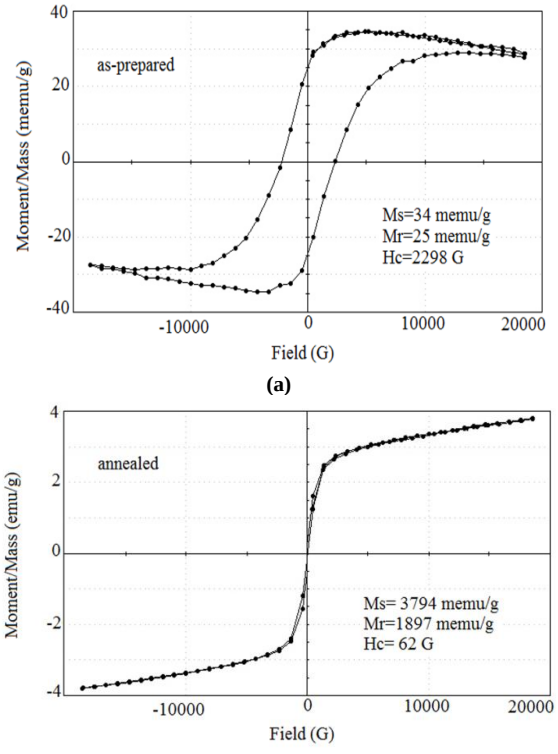

Fig. 4. Magnetic measurements (VSM) analysis of (a) as-prepared and (b) annealed Zinc ferrite samples

Magnetizations M versus applied magnetic field H for samples are measured. Magnetic measurements show a coercive field (Hc) and saturation magnetism (Ms) of 2298 G and 34 memu/g respectively for as-prepared samples while coercive field and saturation magnetism change to 62 G and 3794 memu/g respectively for annealed one at 500 ºC. It may be because of agglomeration and oxidation of the ZnO due to increasing of the Zn^{2+} into the crystal lattice.

Figure 5 shows the fourier transport infrared spectrum (FTIR) analysis of the as-prepared and annealed Zinc ferrite

samples in the range of 400-4000 cm^{-1} frequencies to identify the chemical bonds as well as functional groups in the compound. The large broad band at 3234 cm^{-1} is ascribed to the O-H stretching vibration in OH groups. The absorption peaks at 1620 cm^{-1} and 1421 cm^{-1} are due to the asymmetric and symmetric bending vibration of C=O respectively. The sharp peaks in FTIR spectrum determined the stretching vibrations of Zinc ferrite groups in the frequencies of 675 cm^{-1}, 602 cm^{-1} and 476 cm^{-1}. It seems the intensity of the transmission Zinc ferrite vibration peaks increased after annealing.

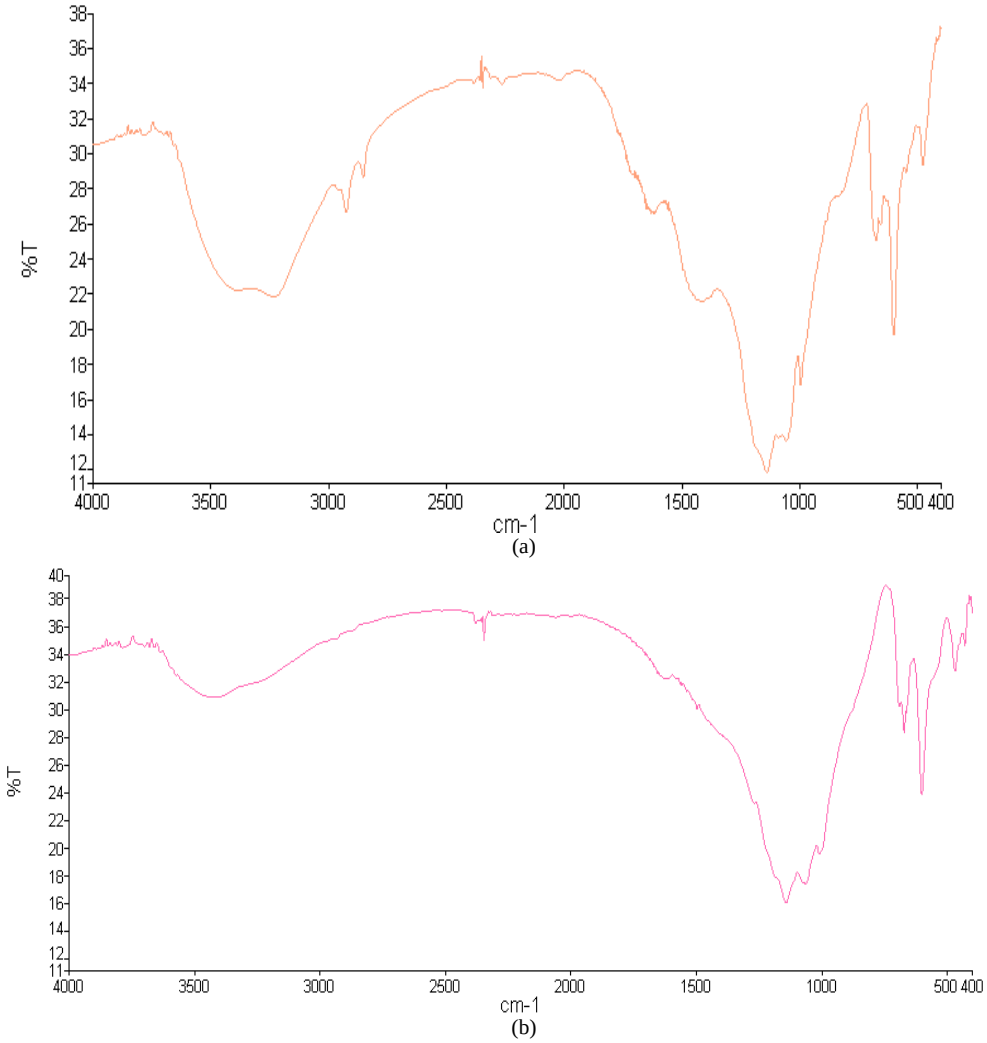

Fig. 5. FTIR spectrum of a) as-prepared and b) annealed Zinc ferrite samples

X-ray florescence analysis (XRF) of Zinc ferrite NPs prepared by solgel synthesis is shown in figure 6. The as-synthesized and annealed $ZnFe_2O_4$ samples affirms the existence of Zn and Fe elements. XRF shows peaks of iron and zinc elements with less Sb, Ag and Bi contaminations. The XRF data revealed decreasing of the Fe weight percent from 41.28 %Wt. to 39.647 %Wt., by annealing samples. It may be because of oxidation of the Fe_2O_3 and decreasing of the Fe^{3+} into the crystal lattice. The ratio of Fe/Zn are determined as 0.712 and 0.693 for as prepared and annealed samples respectively, that shows decreasing of the Fe content because of oxidation after heat treatment.

SUMMARY AND CONCLUSION

The samples were successfully synthesized by solgel method. The XRD spectra showed the rhombohedral Fe_2O_3 and hexagonal wurtzite ZnO structure. The SEM images indicated that the NPs changed from rod-shape to nanoparticle clusters $ZnFe_2O_4$ by increasing temperature. TEM image exhibited the formation of core-shell Zinc ferrite NPs with a diameter of 10 nm Fe_2O_3 shell around them. FTIR analysis indexed the presence of Fe and Zn oxides stretching bound. VSM analysis showed the large magnetization of the samples compared to paramagnetic $ZnFe_2O_4$. It is due to some of the Zn^{2+} ion which is transferred to the octahedral position. Thus the synthesized

$ZnFe_2O_4$ has formed superparamagnetic rather than paramagnetic. The maximum magnetization of annealed samples at 20 kG was found to be 3.8 emu/g with a negligible coercivity of 62 G and a remanence magnetization of 1.9 emu/g. Finally, XRF analysis confirmed decreasing of the Fe content because of oxidation after annealing.

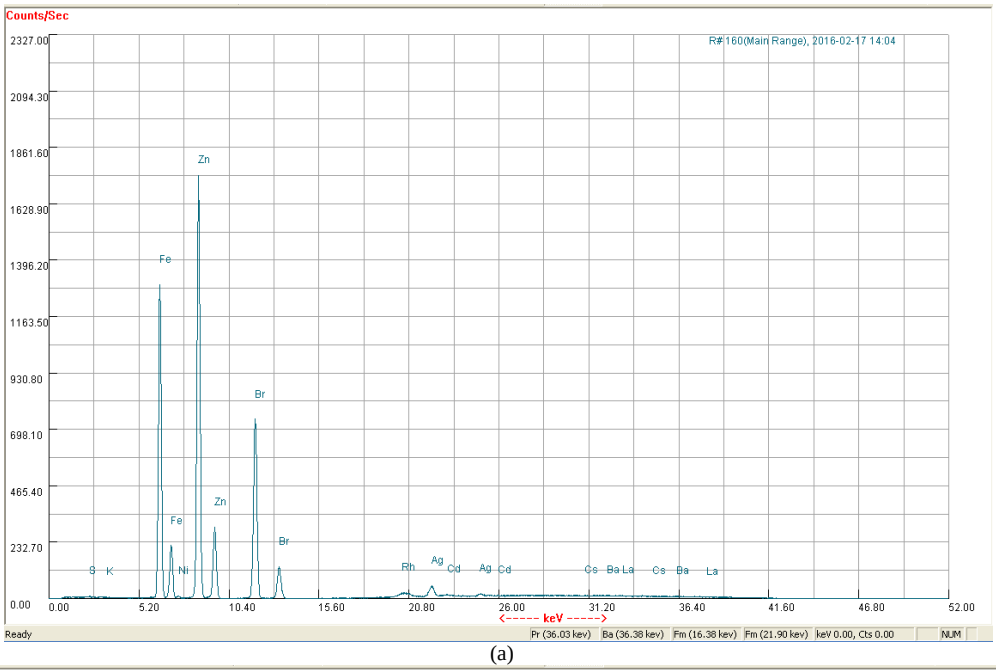

(a)

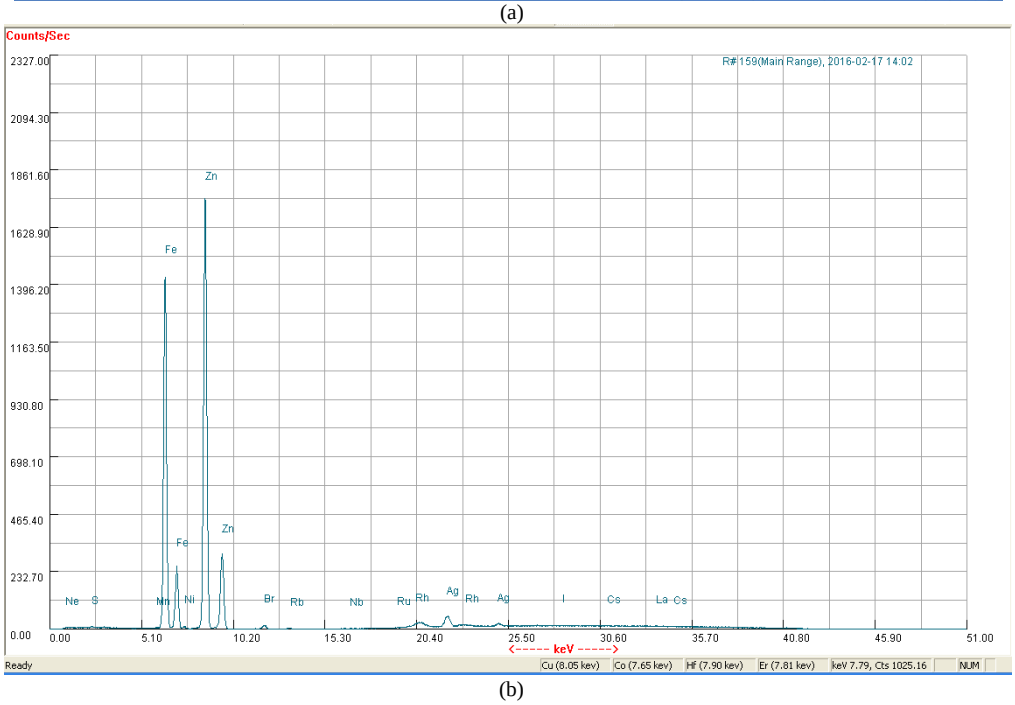

(b)

Fig. 6. XRF analysis of a) as-prepared and b) annealed Zinc ferrite NPs

ACKNOWLEDGMENTS

The authors are thankful for the financial support of varamin pishva branch at Islamic Azad University for analysis and the discussions on the results.

REFERENCES

[1] Dastpak M, Farahmandjou M, Firoozabadi TP. Synthesis and Preparation of Magnetic Fe-Doped CeO_2 Nanoparticles Prepared by Simple Sol-Gel Method.

Journal of Superconductivity and Novel Magnetism. 2016; 29(11): 2925-9.

[2] Farahmandjou M, Soflaee F. Polymer-Mediated Synthesis of Iron Oxide (Fe_2O_3) Nanorods. Chinese Journal of Physics. 2015; 53: 080801.

[3] Zarinkamar M, Farahmandjou M, Firoozabadi TP. Diethylene Glycol-Mediated Synthesis of Nano-Sized Ceria (CeO_2) Catalyst. Journal of Nanostructures. 2016; 6(2): 116-20.

[4] Farahmandjou M. Magnetocrystalline properties of Iron-Platinum ($L1_0$-FePt) nanoparticles through phase transition. Iranian Journal of Physics Research. 2016; 16(1): 1-5.

[5] Shadrokh S, Farahmandjou M, Firozabadi TP. Fabrication and Characterization of Nanoporous Co Oxide (Co_3O_4) Prepared by Simple Sol-gel Synthesis. Physical Chemistry Research. 2016; 4(2): 153-60.

[6] Farahmandjou M, Honarbakhsh S, Behrouzinia S. PVP-Assisted Synthesis of Cobalt Ferrite ($CoFe_2O_4$) Nanorods. Physical Chemistry Research. 2016; 4(4): 655-62.

[7] Farahmandjou M, Soflaee F. Synthesis and characterization of α-Fe_2O_3 nanoparticles by simple co-precipitation method. Physical Chemistry Research. 2015; 3(3); 193-8.

[8] Farahmandjou M. Synthesis and Structural Study of $L1_0$-FePt nanoparticles. Turkish Journal of Engineering and Environmental Sciences. 2011, 34(4), 265-70.

[9] Raizada P, Sudhaik A, Singh P, Hosseini-Bandegharaei A, Gupta VK, Agarwal S. Silver-mediated Bi_2O_3 and graphitic carbon nitride nanocomposite as all solid state Z scheme photocatalyst for imidacloprid pesticide abatement from water. Desalination and water treatment. 2019; 171: 344-55.

[10] Safarifarda V, Morsalib A. Facile preparation of nanocubes zinc-based metal-organic framework by an ultrasound-assisted synthesis method; precursor for the fabrication of zinc oxide octahedral nanostructures. Ultrasonics sonochemistry. 2018; 40: 921-8.

[11] Azimzadeh Asiabi P, Ramazani A, Khoobi M, Amin M, Shakoori M, Mirmohammad Sadegh N, Farhadi R. Regenerated silk fibroin-based dressing modified with carnosine-bentonite nanosheets accelerates healing of second-degree burn wound. Chemical Papers. 2020; 74(10): 3243-57.

[12] Fardood ST, Forootan R, Moradnia F, Afshari Z, Ramazani A. Green synthesis, characterization, and photocatalytic activity of cobalt chromite spinel nanoparticles. Materials Research Express. 2020; 7 (1): 015086

[13] Yana XW, Joharian M, Naghiloo M, Rasuli R, Hud ML, Morsali A. Metal–organic framework derived porous 2D semiconductor C/ZnO nanocomposite with the high electrical conductivity. Materials Letters. 2019; 252: 325-8.

[14] Mehr ES, Sorbiun M, Ramazani A, Taghavi Fardood S. Plant-mediated synthesis of zinc oxide and copper oxide nanoparticles by using ferulago angulata (schlecht) boiss extract and comparison of their photocatalytic degradation of Rhodamine B (RhB) under visible light irradiation. Journal of Materials Science: Materials in Electronics. 2018; 29(2): 1333-40.

[15] Pormazar SM, Ehrampoush MH, Ghaneian MT, Khoobi M, Talebi P, Dalvand A. Application of amine-functioned Fe3O4 nanoparticles with HPEI for effective humic acid removal from aqueous solution: Modeling and optimization",Korean Journal of Chemical Engineering. 2020; 37(1): 93-104.

[16] Ansari A, Vahedi S, Tavakoli O, Khoobi M, Faramarzi MA. Novel Fe3O4/hydroxyapatite/β-cyclodextrin nanocomposite adsorbent: Synthesis and application in heavy metal removal from aqueous solution. Applied Organometallic Chemistry. 2019; 33(1): e4634.

[17] Atrak K, Ramazani A, Taghavi Fardood S. Eco-friendly synthesis of Mg0.5Ni0.5AlxFe2-xO4 magnetic nanoparticles and study of their photocatalytic activity for degradation of direct blue 129 dye. Journal of Photochemistry and Photobiology A: Chemistry. 2019; 382: 111942,.

[18] Zarekarizi F, Beheshti S, Morsali A. Solid-state preparation of mixed metal-oxides nanostructure from anionic metal-organic framework via cation exchange process. Inorganic Chemistry Communications. 2018; 97: 144-8.

[19] Taghavi Fardood S, Moradnia F, Ramazani A. Green synthesis and characterisation of ZnMn2O4 nanoparticles for photocatalytic degradation of Congo red dye and kinetic study. Micro & Nano Letters, 2019; 14(9): 986-91.

[20] Masoomi MY, Beheshti S, Morsali A. Shape Control of Zn(II) Metal–Organic Frameworks by Modulation Synthesis and Their Morphology-Dependent Catalytic Performance. Ultrasonics sonochemistry. 2018; 45, 197-203.

[21] Moradnia F, Ramazani A, Taghavi Fardood S, Gouranlou F. A novel green synthesis and characterization of tetragonal-spinel $MgMn_2O_4$ nanoparticles by tragacanth gel and studies of its photocatalytic activity for degradation of reactive blue 21 dye under visible light. Materials Research Express. 2019; 6(7): 075057.

[22] Hayati P, Suárez-García S, Gutierrez A, Şahin E, Molina DR, Morsali A, Rezvania AR. Sonochemical synthesis of two novel Pb (II) 2D metal coordination polymer complexes: New precursor for facile fabrication of lead (II) oxide/bromide micro-nanostructures. Ultrasonics sonochemistry. 2017; 42: 310-9.

[23] Yeganeh MS, Kazemizadeh AR, Ramazani A, Eskandari P, Angourani HR. Plant-mediated synthesis

of Cu0.5Zn0.5Fe2O4 nanoparticles using Minidium leavigatum and their applications as an adsorbent for removal of reactive blue 222 dye. Materials Research Express. 2020; 6(12): 1250f4.

[24] Mohammadi M, Khazaei A, Rezaei A, Huajun Z, Xuwei S. Ionic-Liquid-Modified Carbon Quantum Dots as a Support for the Immobilization of Tungstate Ions (WO42–): Heterogeneous Nanocatalysts for the Oxidation of Alcohols in Water. ACS Sustainable Chemistry & Engineering. 2019; 7(5): 5283-91.

[25] Azari BE, Ramazani A, Fardood ST, Morsali A. Green synthesis and characterization of ZnAl2O4@ZnO nanocomposite and its environmental applications in rapid dye degradation. Optik. 2020; 208: 164129.

[26] Gholibegloo E, Karbasib A, Pourhajibagher M, Chiniforush N, Ramazani A, Akbari T, Bahador A, Khoobi M. Carnosine-graphene oxide conjugates decorated with hydroxyapatite as promising nanocarrier for ICG loading with enhanced antibacterial effects in photodynamic therapy against Streptococcus mutans. Journal of Photochemistry and Photobiology B: Biology. 2018; 181: 14-22.

[27] Yaghoubi A, Ramazani A. Anticancer DOX delivery system based on CNTs: Functionalization, targeting and novel technologies. Journal of Controlled Release. 2020; 327: 198-224.

[28] Wang R, Gan J, Li R, Duan J, Zhou J, Lv M, Qi R. Controlled delivery of ketamine from reduced graphene oxide hydrogel for neuropathic pain: In vitro and in vivo studies", Journal of Drug Delivery Science and Technology. 2020; 60: 101964.

[29] Kamani H, Nasseri S, Nabizadeh R, Khoobi M, Ashrafi D, Bazrafshan E, Mahvi AH. Sonocatalytic oxidation of reactive blue 29 by N-doped TiO2 from aqueous solution. Journal of Mazandaran University of Medical Sciences. 28(166):157-69.

[30] Moradniaa F, Fardood ST, Ramazani A,Guptac VK. Green synthesis of recyclable MgFeCrO4 spinel nanoparticles for rapid photodegradation of direct black 122 dye. Journal of Photochemistry and Photobiology A: Chemistry. 2020; 392: 112433.

[31] Mohammadi M, Rezaei A, Khazaei A, Xuwei S, Huajun Z. Targeted Development of Sustainable Green Catalysts for Oxidation of Alcohols via Tungstate-Decorated Multifunctional Amphiphilic Carbon Quantum Dots. ACS applied materials & interfaces. 2019; 11(36): 33194-206.

[32] Zhang NN, Bigdeli F, Miao Q, Hu ML, Morsali A. Ultrasonic-assisted synthesis, characterization and DNA binding studies of Ru(II) complexes with the chelating N-donor ligand and preparing of RuO2 nanoparticles by the easy method of calcinations. Journal of Organometallic Chemistry. 2018; 878: 11-8.

[33] Manafi A, Hosseini M, Fakhri A, Gupta VK, Agarwal S. Investigation of photocatalytic process for iron disulfide-bismuth oxide nanocomposites by using response surface methodology: Structural and antibacterial properties. Journal of Molecular Liquids. 2019; 289: 110950.

[34] Mortezazadeh T, Gholibegloo E, Riyahi Alam N, Haghgoo S, Musa AE, Khoobi M. Glucosamine Conjugated Gadolinium (III) Oxide Nanoparticles as a Novel Targeted Contrast Agent for Cancer Diagnosis in MRI. Journal of Biomedical Physics and Engineering. 2020; 10(1): 25-38.

[35] Xue JJ, Bigdeli F, Liu JP, Hu ML, Morsali A. Ultrasonic-assisted synthesis and DNA interaction studies of two new Ru complexes; RuO2 nanoparticles preparation. Nanomedicine. 2018; 13(21): 2691-708.

[36] Farahmandjou M, Honarbakhsh S, Behrouzinia S. FeCo Nanorods Preparation Using New Chemical Synthesis. Journal of Superconductivity and Novel Magnetism. 2018; 31: 4147-52.

[37] Farahmandjou M, Dastpak M. Fe-Loaded CeO_2 Nanosized Prepared by Simple Co-Precipitation Route. Physical Chemistry Research. 2018; 6(4) 713-20.

[38] Farahmandjou M, Motaghi S. Sol-gel Synthesis of Ce-doped α-Al_2O_3: Study of Crystal and Optoelectronic Properties. Optics Communications. 2019; 441: 1-7.

[39] Motaghi S, Farahmandjou M. Structural and optoelectronic properties of Ce-Al_2O_3 nanoparticles prepared by sol-gel precursors. Material Research Express. 2019; 6(4): 045008.

[40] Farahmandjou M. Synthesis of ITO Nanoparticles Prepared by Degradation of Sulfide Method. Chinese Physics Letter. 2012; 29(7): 077306.

[41] Farahmandjou M, Golabiyan N. Synthesis and characterization of Alumina (Al_2O_3) nanoparticles prepared by simple sol-gel method. International Journal of Bio-Inorganic Hybrid Nanomaterials. 2016; 5(1): 73-7.

[42] Farahmandjou M, Golabiyan N. Solution combustion preparation of nano-Al_2O_3: Synthesis and characterization. Transport Phenomena in Nano and Micro Scales. 2015; 3(2): 100-5.

[43] Farahmandjou M, Golabiyan N. New pore structure of nano-alumina (Al_2O_3) prepared by sol gel method. Journal of Ceramic Processing Research. 2015; 16(2): 1-4.

[44] Khodadadi A, Farahmandjou M, Yaghoubi M, Amani AR. Structural and Optical Study of Fe^{3+}-Doped Al_2O_3 Nanocrystals Prepared by New Sol gel Precursors. International Journal of Applied Ceramic Technology. 2019; 16(2): 718-26.

[45] Farahmandjou M. The study of electro-optical properties of nanocomposite ITO thin films prepared by e-beam evaporation. Revista mexicana de física. 2013; 59(3): 205-7.

[46] Zarinkamar M, Farahmandjou M, Firoozabadi TP. One-step synthesis of ceria (CeO_2) nano-spheres by a simple wet chemical method. Journal of Ceramic Processing Research. 2016; 17(3): 166-9.

[47] Khodadadi A, Farahmandjou M, Yaghoubi M. Investigation on synthesis and characterization of Fe-doped Al_2O_3 nanocrystals by new sol–gel precursors. Materials Research Express. 2019; 6: 025029.

[48] Farahmandjou M, Zarinkamar M. Synthesis of nano-sized ceria (CeO_2) particles via a cerium hydroxy carbonate precursor and the effect of reaction temperature on particle morphology. Journal of Ultrafine Grained Nanostructured Materials. 2015; 48(1): 5-10.

[49] Farahmandjou M, Zarinkamar M, Firoozabadi TP. Synthesis of Cerium Oxide (CeO_2) nanoparticles using simple Co-precipitation method. Revista mexicana de física. 2016; 62(5): 496-9.

[50] Farahmandjou M, Salehizadeh SA. The optical band gap and the tailing states determination in glasses of TeO_2-V_2O_5-K_2O system, Glass Physics and Chemistry. 2013; 39(5): 473-9.

[51] Behrouzinia S, Salehinia D, Khorasani K, Farahmandjou M. The continuous control of output power of a CuBr laser by a pulsed external magnetic field. Optics Communications. 2019; 436: 143-5.

[52] Farahmandjou M. Effect of Oleic Acid and Oleylamine Surfactants on the Size of FePt Nanoparticles. Journal of Superconductivity and Novel Magnetism. 2012; 25(6): 2075–9.

[53] Hoseini F, Farahmandjou M, Firoozabadi TP. Coprecipitation synthesis of zinc ferrit (FE_2O_3/ZNO) nanoparticles prepared by CTAB surfactant. Journal of Fundamental and Applied Sciences. 2016: 8(3): 738-45.

[54] Farahmandjou M, Soflaee F. Synthesis of Iron Oxide Nanoparticles using Borohydride Reduction, Journal of Bio-Inorganic Hybrid Nanomaterials. 2014; 3(4): 203-6.

[55] Honarbakhsh S, Farahmandjou M, Behroozinia S. Synthesis and characterization of iron cobalt (FeCo) nanorods prepared by simple Co-precipitation method. Journal of Fundamental and Applied Sciences. 2016; 8(2): 892-900.

[56] Sebt SA, Parhizgar SS, Farahmandjou M, Aberomand P, Akhavan M. The role of ligands in the synthesis of FePt nanoparticles, Journal of Superconductivity and Novel Magnetism. 2009; 22(8): 849-54.

[57] Farahmandjou M, Sebt SA, Parhizgar SS, Aberomand P, Akhavan M. Stability investigation of colloidal FePt nanoparticle systems by spectrophotometer analysis. Chinese Physics Letter. 2009; 26(2): 027501.

[58] Jurablu S, Farahmandjou M, Firoozabadi TP. Multiple-layered structure of obelisk-shaped crystalline nano-ZnO prepared by sol–gel route. Journal of Theoretical and Applied Physics. 2015; 9(4): 261-6.

[59] Farahmandjou M, Ramazani M. Fabrication and Characterization of Rutile TiO_2 Nanocrystals by Water Soluble Precursor. Physical Chemistry Research. 2015; 3(4): 293-8.

[60] Akhtari F, Zorriasatein S, Farahmandjou M, Elahi SM. Structural, optical, thermoelectrical, and magnetic study of $Zn_{1-x}Co_xO$ ($0 \leq x \leq 0.10$) nanocrystals. Int. International Journal of Applied Ceramic Technology. 2018; 15(3): 723-33.

[61] Akhtari F, Zorriasatein S, Farahmandjou M, Elahi SM. Synthesis and optical properties of Co^{2+}-doped ZnO Network prepared by new precursors. Materials Research Express. 2018; 5(6): 065015.

[62] Khoshnevisan B, Marami MB, Farahmandjou M. Fe^{3+}-Doped Anatase TiO_2 Study Prepared by New Sol-Gel Precursors. Chinese Physics Letter. 2018; 35(2): 027501.

[63] Marami MB, Farahmandjou M, Khoshnevisan B. Solgel Synthesis of Fe-doped TiO_2 Nanocrystals. Journal of Electronic Materials. 2018; 47(7): 3741-8.

[64] Farahmandjou M, Khalili P. Study of Nano SiO_2/TiO_2 Superhydrophobic Self-Cleaning Surface Produced by Sol-Gel. Australian Journal of Basic and Applied Sciences. 2013; 7(6): 462-5.

[65] Jurablu S, Farahmandjou M, Firoozabadi TP. Sol-gel synthesis of zinc oxide (ZnO) nanoparticles: study of structural and optical properties. Journal of Science, Islamic Republic of Iran. 2015; 26(3): 281-5.

[66] Farahmandjou M, Khalili P. Morphology Study of anatase nano-TiO_2 for Self-cleaning Coating. International Journal of Fundamental Physical Sciences. 2013; 3(3): 54-6.

[67] Jafari A, Khademi S, Farahmandjou M. Nano-crystalline Ce-doped TiO_2 Powders: Sol-gel Synthesis and Optoelectronic Properties. Materials Research Express. 2018; 5(9): 095008..

[68] Jafari A, Khademi S, Farahmandjou M, Darudi A, Rasuli R. Structural and optical properties of Ce^{3+}-doped TiO_2 nanocrystals prepared by sol-gel precursors. Journal of Electronic Materials. 2018; 47(11): 6901-8.

[69] Marami MB, Farahmandjou M. Water-Based Sol–Gel Synthesis of Ce-Doped TiO_2 Nanoparticles, Journal of Electronic Materials. 2019; 48(7): 4740-7.

[70] Ramazani M, Farahmandjou M, Firoozabadi TP. Effect of nitric acid on particle morphology of the nano-TiO_2. International Journal of Nanoscience and Nanotechnology. 2015; 11(2): 115-22.

[71] Mohapatra J, Mitra A, Bahadur D, Aslam M. Surface controlled synthesis of MFe_2O_4 (M=Mn, Fe, Co, Ni and Zn) nanoparticles and their magnetic characteristics. Crystal Engineering Communication. 2013; 15: 524-32.

[72] Zhou Z, Zhu X, Wu D, ChenQ, Huang D, Sun C, Xin J, Ni K, Gao J. Anisotropic Shaped Iron Oxide Nanostructures: Controlled Synthesis And Proton Relaxation Shortening Effects. Chemistry of Materials. 2015; 27: 3505-15

[73] Mohapatra J, Mitra A, Tyagi H, Bahadur D, Aslam M. Iron oxid enanorodsas high-performance magnetic

resonance imaging contrast agents. Nanoscale. 2015; 79174-84.

[74] Manjura Hoque S, Sazzad Hossain MD, Choudhury S, Akhter S, Hyder F. Synthesis and characterization of $ZnFe_2O_4$ nanoparticles and its biomedical applications. Materials Letters. 2016; 162: 60-3.

[75] Scherrer P, Bestimmung der Grosse und der Inneren Struktur von Kolloidteilchen Mittels Rontgenstrahlen, Nachrichten von der Gesellschaft der Wissenschaften. Gottingen. Mathematisch-Physikalische Klasse. 1918; 2: 98-100.

[76] Farahmandjou M, Khodadadi A, Yaghoubi M. Low Concentration Iron-Doped Alumina (Fe/Al_2O_3) Nanoparticles Using Co-Precipitation Method. Journal of Superconductivity and Novel Magnetism. (2020).

[77] Farahmandjou M, Dastpak M. Synthesis of Fe-doped CeO_2 Nanoparticles Prepared by Solgel Method. Journal of Sciences, Islamic Republic of Iran. 2020; 31(1): 39-43.

[78] Farahmandjou M, Khodadadi A, Yaghoubi M. Synthesis and Characterization of $Fe\text{-}Al_2O_3$ nanoparticles Prepared by Coprecipitation Method. Iranian Journal of Chemistry and Chemical Engineering. (2021).

[79] Jafari A, Khademi S, Farahmandjou M, Darudi A, Rasuli R. Preparation and Characterization of Cerium Doped Titanium Dioxide Nanoparticles by the Electrical Discharge Method. Journal of Advanced Materials in Engineering. 2019; 38(2): 83-90.

[80] Farahmandjou M, Golabiyan N. Synthesis and characterisation of Al_2O_3 nanoparticles as catalyst prepared by polymer co-precipitation method. Materials Engineering Research. 2019; 1(2): 40-4.

[81] Farahmandjou M. One-step synthesis of TiO_2 nanoparticles using simple chemical technique. Materials Engineering Research. 2019; 1(1): 15-9.

[82] Moghimi A, Farahmandjou M. Preconcentration of Cd (II) by chemically converted graphene sheets adsorbed on surfactant-coated C18 before determination by flame atomic absorption spectrometry (FAAS). African Journal of Pure and Applied Chemistry. 2014; 8(1): 1-8.

[83] Farahmandjou M. Self-cleaning measurement of nano-sized photoactive TiO_2. Journal of Computer & Robotics. 2014; 7 (2): 15-9.

[84] Farahmandjou M, Abaeyan N. Simple Synthesis of Vanadium Oxide (V_2O_5) Nanorods in Presence of CTAB Surfactant. Colloid Surface Science. 2016; 1(1): 10-3.

[85] Farahmandjou M, Sebt SA, Parhizgar SS, Aberomand P, Akhavan M. The Effect of NaCl Prepared by Ultra-sonic Vibration on the Sintering of Annealed FePt Nanoparticles. Journal of Physics: Conference Series. 2009; 153(1): 012050.

[86] Farahmandjou M. Liquid Phase Synthesis of indium tin oxide (ITO) nanoparticles using In (III) and Sn (IV) salts. Australian Journal of Basic and Applied Sciences. 2013; 7(4): 31-4.

[87] Farahmandjou M. Comparison of the Fe and Pt nanoparticles with FePt alloy prepared by polyol process: Shape and composition study. Acta Physica Polonica A. 2013; 123: 277-8.

[88] Farahmandjou M. The effect of reflux process on the size and uniformity of FePt nanoparticles. International Journal of fundamental physical sciences. 2011; 1(3): 57-9.

[89] Farahmandjou M. Synthesis and Morphology Study of Nano-Indium Tin Oxide (ITO) Grains. International Journal of Bio-Inorganic Hybrid Nanomaterials. 2013; 2(2), 373-8.

[90] Farahmandjou M, Jurablu S. Co-precipitation Synthesis of Zinc Oxide (ZnO) Nanoparticles by Zinc Nitrate Precursor. Journal of Bio-Inorganic Hybrid Nanomaterials. 2014; 3(3): 179-84.

[91] Farahmandjou M, Salehizadeh SA. Investigation on calorimetric and elastic properties of $50TeO_2$-(50-x) V_2O_5-xK_2O glassy systems. Chalcogenide Letters. 2015; 12(11): 619-31.

[92] Farahmandjou M, Abaeiyan N. Chemical synthesis of vanadium oxide (V_2O_5) nanoparticles prepared by sodium metavanadate. Journal of Nanomedicine Research. 2017; 5(1): 00103.

[93] Farahmandjou M, Abaeiyan N. Simple synthesis of new nano-sized pore structure vanadium pantoxide (V_2O_5). Journal of Bio-Inorganic Hybrid Nanomaterials. 2015; 4(4): 243-7.

[94] Farahmandjou M, Shadrokh S. Chemical synthesis of the Co_3O_4 nanoparticles in presence of CTAB surfactant. Journal of Bio-Inorganic Hybrid Nanomaterials. 2015; 4(3): 129-34.

[95] Behrouzinia S, Khorasani K, Farahmandjou M. Buffer gas effects on output power of a copper vapor laser. Laser Physics. 2016; 26(5): 055003.

[96] Farahmandjou M, Behrouzinia S. Fe Lauded TiO_2 Nanoparticles Synthesized by Sol-gel Precursors. Physical Chemistry Research. 2019; 7(2): 395-401.

[97] Farahmandjou M., Khodadadi A, Yaghoubi M. Low Concentration Iron-Doped Alumina (Fe/Al_2O_3) Nanoparticles Using Co-Precipitation Method. Journal of Superconductivity and Novel Magnetism. (2020).

[98] Farahmandjou M, Dastpak M, Panji Z. CTAB-assisted of Fe_2O_3/CeO_2 nanosized prepared by coprecipitation method. Journal of Bio-Inorganic Hybrid Nanomaterials. 2018; 7(3): 221-6.

[99] Farahmandjou M. The Effect of 1, 2-Hexadecadeniol and $LiBEt_3H$ Superhydride on the Size of FePt Nanoparticles. AIP Conference Proceedings. 2011; 1415(1): 193-5.

[100] Farahmandjou M. Shape and composition study of iron-platinum (FePt) nanoalloy prepared by polyol process. International Journal of Physical Sciences. 2012; 7(12): 1938-42.

[101] Farahmandjou M. Two step growth process of iron-platinum (FePt) nanoparticles. International Journal of Physical Sciences. 2012; 7(19): 2713-19.

[102] Farahmandjou M. Preparation of Ferromagnetic Co_3O_4 Nanoparticles by Wet Chemical Synthesis Method. To Physics Journal. 2019; 3: 89-99.